JVI Journals.ASM.org

A Vaccinia Virus-Driven Interplay between the MKK4/7-JNK1/2 Pathway and Cytoskeleton Reorganization

Anna C. T. C. Pereira,[a,b*] Flávia G. G. Leite,[a,b*] Bruno S. A. F. Brasil,[a,b*] Jamaria A. P. Soares-Martins,[c] Alice A. Torres,[a,b] Paulo F. P. Pimenta,[d] Thaïs Souto-Padrón,[e] Paula Traktman,[c] Paulo C. P. Ferreira,[b] Erna G. Kroon,[b] and Cláudio A. Bonjardim[a,b]

Grupo de Transdução de Sinal/Orthopoxvirologia[a] and Laboratório de Vírus,[b] Departamento de Microbiologia, Instituto de Ciências Biológicas, Universidade Federal de Minas Gerais, Minas Gerais, Belo Horizonte, Brazil; Department of Microbiology and Molecular Genetics, Medical College of Wisconsin, Milwaukee, Wisconsin, USA[c]; Centro de Pesquisa René Rachou, Belo Horizonte, Minas Gerais, Brazil[d]; and Laboratório de Biologia Celular e Ultraestrutura, Instituto Nacional de Ciência e Tecnologia em Biologia Estrutural e Bioimagens, Universidade Federal do Rio de Janeiro, Rio de Janeiro, Brazil[e]

Viral manipulation of transduction pathways associated with key cellular functions such as survival, response to microbial infection, and cytoskeleton reorganization can provide the supportive milieu for a productive infection. Here, we demonstrate that vaccinia virus (VACV) infection leads to activation of the stress-activated protein kinase (SAPK)/extracellular signal-regulated kinase (ERK) 4/7 (MKK4/7)–c-Jun N-terminal protein kinase 1/2 (JNK1/2) pathway; further, the stimulation of this pathway requires postpenetration, prereplicative events in the viral replication cycle. Although the formation of intracellular mature virus (IMV) was not affected in MKK4/7- or JNK1/2-knockout (KO) cells, we did note an accentuated deregulation of microtubule and actin network organization in infected JNK1/2-KO cells. This was followed by deregulated viral trafficking to the periphery and enhanced enveloped particle release. Furthermore, VACV infection induced alterations in the cell contractility and morphology, and cell migration was reduced in the JNK-KO cells. In addition, phosphorylation of proteins implicated with early cell contractility and cell migration, such as microtubule-associated protein 1B and paxillin, respectively, was not detected in the VACV-infected KO cells. In sum, our findings uncover a regulatory role played by the MKK4/7-JNK1/2 pathway in cytoskeleton reorganization during VACV infection.

The *Orthopoxvirus Vaccinia virus* (VACV) is a large DNA virus, approximately 200 kbp, whose replication takes place in the cytoplasm of infected cells. The virus is capable of infecting a wide range of hosts, including rodents and humans, though its natural reservoir remains unknown (7, 20).

It is becoming increasingly apparent that the intracellular environment must present an array of adequate conditions in order to allow productive viral replication (19). In this regard, manipulation of a given pathway by poxviruses may benefit the virus and improve its replication efficiency, as demonstrated by VACV recruitment of the MEK/extracellular signal-regulated kinase (ERK) pathway during replication (1, 9). On the other hand, certain cellular conditions may simply restrict viral replication, as it has been demonstrated that the myxoma virus (MYXV)-stimulated ERK/interferon regulatory factor 3/beta interferon cascade impedes this rabbit-specific virus from replicating in rodent cells (36).

A subfamily of mitogen-activated protein kinases (MAPKs) known as stress-activated protein kinases (SAPKs) encompasses the p38/MAPKs and c-Jun N-terminal kinases (JNKs) (reviewed in references 6, 8, and 44). JNKs and p38/MAPKs are downstream effectors of the Rho family GTPases, which also includes Rac and Cdc42, and they propagate signals associated with a wide spectrum of different, yet overlapping, biological responses, including survival, proliferation, microbial infection, cell migration, and cytoskeleton reorganization. The signal transduction pathway leading to JNK activation, downstream of Rho GTPases, is dependent upon dual phosphorylation carried out by the MAPKs SAPK/ERK 4 (MKK4) and MKK7 on Thr183/Tyr185 of JNK (reviewed in references 2, 13, 23, and 25).

In accordance with these reports, it has been shown that JNK phosphorylates its downstream substrate paxillin at serine 178, and expression of a mutant form of paxillin, Pax S178A, inhibits the migration of various cell lines (13, 14). Accumulating evidence has also implicated JNK in the phosphorylation of microtubule-associated protein 2 (MAP2) and MAP-1B, which are known to regulate microtubule (MT) stabilization and neuronal migration (5, 18). Furthermore, it has been shown that MAP-1B not only binds actin stress fibers (31) but also associates with MTs in a phosphorylation-dependent manner (33). Rho GTPases have also been demonstrated to play a pivotal role in the regulation of both MT dynamics and the actin cytoskeleton (10, 39, 40). Thus, a coordinated regulation of both MT and the actin cytoskeleton allows the cells to deal with diverse biological demands in which the reorganization of both elements is required, such as in cell migration and cell division (41).

There are two infectious forms of VACV: intracellular mature virus (IMV) and extracellular enveloped virus (EEV). IMVs represent 80 to 90% of the viral progeny. They remain inside the cells and are released upon cell lysis (20). After IMV formation in the

Received 4 August 2011 **Accepted** 14 October 2011

Published ahead of print 26 October 2011

Address correspondence to Claudio A. Bonjardim, claudio.bonjardim@pq.cnpq.br.

* Present address: Anna C. T. C. Pereira, Universidade Federal do Piauí, UFPI, Campus Ministro Reis Velloso, Parnaíba, PI, Brazil; Flávia G. G. Leite, Institute of Science and Technology Austria, Am Campus 1, Klosterneuburg, Austria; Bruno S. A. F. Brasil, Universidade Federal de Minas Gerais, UFMG, Escola de Veterinária, Belo Horizonte, MG, Brazil.

A.C.T.C.P., F.G.G.L., and B.S.A.F.B. contributed equally to this article.

Copyright © 2012, American Society for Microbiology. All Rights Reserved.

doi:10.1128/JVI.05638-11

viral factories (VFs), a small subset of the infectious progeny is transported by a microtubule motor (MTM) to the trans-Golgi apparatus, where they are enveloped by a double membrane and referred to as the intracellular enveloped virus (IEV) (30). It has been shown that IEV formation, but not IMV formation, is strictly dependent on an intact MT network, since IEV assembly is impaired when the infection is carried out in the presence of nocodazole, an MT-depolymerizing agent (21). Once assembled, IEV is transported by the MTM to the cell periphery, and its outermost membrane then fuses with the cell membrane to form the cell-associated enveloped virus (CEV), which remains associated with the external cell surface (11, 24, 38).

Although activation of JNK upon VACV infection has been the focus of recent studies (12, 45), the role that JNK1/2 may have in VACV-stimulated cytoskeleton reorganization has not been elucidated. In the present study, we demonstrated that the MKK4/7-JNK1/2 pathway is stimulated in an early-late manner during VACV infection and this event plays a role in both early cell contractility and cell migration.

MATERIALS AND METHODS

Cell culture, antibodies, and chemicals. Mouse embryonic fibroblasts (MEFs) from wild-type (WT), MKK4$^{-/-}$-knockout (KO), MKK7$^{-/-}$-KO, MKK4/7$^{-/-}$-double-KO, and JNK1/2$^{-/-}$-double-KO mice (8, 32), A31 cells (A31 is a clone derived from mouse BALB/c 3T3 cells), as well as BSC-40 cells were cultured in Dulbecco's modified Eagle's medium (DMEM) supplemented with 5% (MEFs), 6% (BSC-40), or 7.5% (A31) (vol/vol) heat-inactivated fetal bovine serum (FBS) (Cultilab, Campinas, SP, Brazil) and antibiotics in 5% CO_2 at 37°C. When needed, cells were starved at 80 to 90% confluence in 1% FBS-DMEM and incubated for 12 h prior to VACV infection. Rabbit polyclonal anti-phospho-JNK1/2 (Thr183/Tyr185) and -c-JUN (Ser 73) antibodies, rabbit polyclonal anti-total ERK1/2 antibody, and antirabbit and antimouse secondary antibodies were purchased from Cell Signaling Technology (Beverly, MA). Rabbit polyclonal anti-phospho-MAP-1B (P-LC1-SMI31) and -paxillin (Ser 178) were purchased from Covance and Bethyl Laboratories, Inc., respectively. Mouse monoclonal anti-β-actin and anti-β-tubulin antibodies as well as 4′,6-diamino-2-phenylindole (DAPI) and cytosine arabinoside (araC) were purchased from Sigma (São Paulo, Brazil). Mouse polyclonal anti-c-Myc antibody was purchased from Santa Cruz Technology. The pharmacological inhibitor JNK inhibitor VIII [JNKi; *N*-(4-amino-5-cyano-6-ethoxypyridin-2-yl)-2-(2,5-dimethoxyphenyl)acetamide] was purchased from Calbiochem-Merck (Darmstadt, Germany). Rhodamine-conjugated phalloidin, rhodamine-conjugated antirabbit and antimouse secondary antibodies, and fluorescein isothiocyanate (FITC)-conjugated antimouse secondary antibody were purchased from Invitrogen-Molecular Probes (Carlsbad, CA). Lipofectamine LTX was purchased from Invitrogen (Carlsbad, CA). The antibody against the viral protein I3 was previously described (24a).

Viruses. (i) Viral stock. Wild-type VACV (strain WR) and the recombinant VACV vF13L-green fluorescent protein (GFP) chimera were propagated in BSC-40 cells and purified by sucrose gradient sedimentation as described previously (15, 16). The experiments presented in this study were carried out with the IMV form of VACV, unless otherwise stated.

(ii) UV-irradiated virus. Viral stocks were exposed for 5 to 15 min to a UV lamp producing irradiation predominantly at 254 nm. UV-irradiated viruses were then tested for infectivity. Viruses unable to form plaques or in which late viral gene expression could not be detected by Western blotting were considered UV inactivated. Cells that were 80 to 90% confluent were infected with VACV in the absence of FBS at the indicated multiplicity of infection (MOI) for the times shown.

(iii) Plaque assays. The viral plaque assays were performed as described previously (4). Briefly, confluent BSC-40 cells grown on 6-well plates were infected with VACV in 10-fold serial dilutions. Cells were incubated for 1 h adsorption at 37°C, and the titers were determined by counting plaques at 48 h postinfection (hpi), when cells were fixed and stained with 10% formaldehyde and crystal violet.

Viral yield assays. WT, JNK1/2-KO, and MKK4/7-KO cells were cultured and starved as stated above at a density of 4×10^5 cells per well in a 6-well culture dish and then infected with VACV. For the multistep viral growth, infections of WT and JNK1/2-KO cells were carried out at an MOI of 10 for 3, 6, 12, 24, 36, and 48 h. For evaluation of one-step virus growth, infections of WT cells, WT cells with JNKi, and MKK4/7-KO cells were performed at an MOI of 10 for 24 h. Cultures were then washed with cold phosphate-buffered saline (PBS), and cells were lysed by freeze-thaw. The virus was collected from the supernatant of centrifuged cells, and the viral yield was quantitated by plaque assay on BSC-40 cells as described above. For the titration of EEV released from infected cells, triplicates of culture supernatants of WT and JNK-KO cells infected with VACV at an MOI of 10 for 36 h were incubated with anti-IMV-specific antibody, L1R (1:1,000), at 37°C for 1 h and also titrated on BSC-40 cells. The results are presented as the averages of duplicate experiments. Statistical analysis by two-tailed Student's *t* test was performed with ABI Prism (version 3.0) software.

Viral plaque size. WT and JNK-KO cells, at a density of 4×10^5 cells per well in a 6-well culture dish, were infected with 10-fold serial dilutions of VACV WR in medium lacking or supplemented with 1.0% agarose. At 72 hpi, cells were fixed with 10% formaldehyde and stained with 0.3% (wt/vol) crystal violet, and the plaque phenotype was analyzed.

Western blotting. (i) Lysate preparation. Cells were grown and starved as stated above and then infected with VACV at an MOI of 10 for the indicated times. To evaluate the effect of the pharmacological inhibitor JNKi on virus-stimulated JNK1/2 activation, cells were incubated with the indicated concentrations of the inhibitor for 30 min prior to virus infection. Cells were washed twice with ice-cold PBS and lysed on ice with lysis buffer (100 mM Tris-HCl [pH 8.0], 1% Triton X-100, 0.2 mM EDTA, 20% glycerol [vol/vol], 200 mM NaCl, 1 mM $NaVO_3$ [sodium orthovanadate], 1 mM phenylmethylsulfonyl fluoride [PMSF], 5 μg/ml aprotinin, 2.5 μg/ml leupeptin, 1 mM dithiothreitol). Lysates were scraped and collected into Eppendorf tubes and then centrifuged at 13,500 rpm for 15 min at 4°C. Protein concentration was determined using the Bio-Rad assay.

(ii) Electrophoresis and immunoblotting. Forty micrograms of the whole-cell extract (WCE) per sample was separated by electrophoresis on a 10% SDS-polyacrylamide gel and transferred onto nitrocellulose membranes as described previously (9). Membranes were blocked at room temperature for 1 h with PBS containing 5% (wt/vol) nonfat milk and 0.1% Tween 20. The membranes were washed three times with PBS containing 0.1% Tween 20 and incubated with specific rabbit polyclonal anti-phospho-JNK1/2 (1:1,000), anti-total ERK1/2 (1:1,500), anti-phospho-JUN (1:1,000), or mouse monoclonal anti-β-actin (1:5,000) antibodies in PBS containing 5% (wt/vol) bovine serum albumin (BSA) and 0.1% Tween 20. After washing, the membranes were incubated with horseradish peroxidase-conjugated antirabbit (1:3,000) or antimouse (1:1,000) secondary antibody. Immunoreactive bands were visualized using an enhanced chemiluminescence detection system as described in the manufacturer's instructions (GE Healthcare, United Kingdom).

Electron microscopy. WT or JNK1/2-KO cells were infected with VACV at an MOI of 2 and incubated at 37°C for 18 h. Cells were fixed with 2.5% glutaraldehyde in 0.1 M phosphate buffer (pH 7.4) for 1 h at room temperature, scraped gently, and collected by centrifugation. Cells were washed with cacodylate buffer and postfixed with 1% osmium tetroxide solution containing 0.8% ferrocyanide and 5 mM calcium chloride in 0.1 M cacodylate buffer (pH 7.2) for 1 h at room temperature. Cells were rinsed in cacodylate buffer, dehydrated in acetone, and embedded in PolyBed 812 resin. Thin sections were examined using an FEI Morgagni transmission electron microscope operating at 80 kV.

Immunofluorescence microscopy. A total of 2×10^4 WT, JNK1/2-KO, and MKK4/7-KO cells were grown on coverslips, serum deprived for

12 h, and infected with VACV WR or with recombinant VACV vF13L-GFP chimera (15) at an MOI of 5. For phospho-JNK localization, BSC-40 cells were transfected by Lipofectamine LTX with pcDNA3-cMyc-JNK2-MKK7, and at 48 h posttransfection, cells were infected with VACV WR at an MOI of 5. All the infections were carried out for the times indicated in the applicable figures, and at each time point, cells were rinsed in cold PBS and fixed with 4% paraformaldehyde (PFA) in PBS for 10 min at room temperature (RT). After fixation, the cells were permeabilized with 0.2% Triton X-100 in 3% BSA–PBS for 5 min, followed by a 30-min incubation at RT with 3% BSA–2% FBS in PBS for blocking. Cells were stained for 1 h at RT with specific primary antibodies: anti-β-tubulin (1:50), anti-B5 (1:400), or anti-c-Myc (1:50). The following antibodies were used as secondary antibodies: rhodamine-conjugated antirabbit secondary antibody (1:400) and FITC-conjugated antimouse secondary antibody (1:100 to 1:200). To visualize the nucleus as well as viral replication factories, cells were stained with DAPI for 15 min at RT. To visualize the actin network, cells were stained with rhodamine-conjugated phalloidin for 30 min at RT. Fluorescently labeled cells were visualized using a Zeiss (LSM 510 META) confocal laser scanning microscope. Images were processed with LSM Image Browser and Adobe Photoshop (version 7.0) software.

Wound-healing assay. For wound-healing experiments, confluent monolayers of WT, JNK1/2-KO, or MKK4/7-KO MEFs were scratched with a pipette tip and VACV WR was added at an MOI of 5 in serum-free medium. Alternatively, WT MEFs were treated with JNKi (4 μM) for 30 min prior to virus infection and incubated in the continuous presence of the inhibitor. Cells were fixed at 0, 6, 12, and 24 h postinfection and processed for microscopic analysis. Phase-contrast images were captured using an Olympus IX70 microscope.

RESULTS

VACV activates JNK1/2 via MKK4 and MKK7. Virus-host cell interactions are frequently associated with alterations that occur in the cytoskeleton and/or in the intracellular environment (22, 37). Cells are equipped with stress-activated protein kinases (SAPKs), which are also known as c-Jun N-terminal kinases (JNKs), to sense and to respond to diverse environmental stresses associated with proinflammatory cytokines, UV radiation, and microbial infections (6, 8, 44). To investigate whether VACV infection could also lead to JNK1/2 stimulation, A31 cells were infected at an MOI of 10 for 3, 6, 12, 24, and 36 h. At each time, cell lysates were collected, subjected to Western blotting, and then probed with anti-phospho-JNK1/2 antibody. As shown in Fig. 1A, JNK1/2 was phosphorylated only during infection (3 to 36 hpi). The earliest time observed for viral stimulation of JNK1/2 phosphorylation was 1 hpi (data not shown). Since MKK4 and MKK7 are associated with the phosphorylation of JNK1/2 in response to a variety of stimuli, we analyzed whether VACV infection of MKK4$^{-/-}$, MKK7$^{-/-}$, and MKK4/7$^{-/-}$ double mutant cell lines could also result in JNK1/2 phosphorylation. For that, cells were infected with VACV at an MOI of 10 for 6, 12, 24, and 36 h, and phosphorylated JNK1/2 were detected with the specific anti-phospho-JNK antibody. Figure 1B (top) shows that in the absence of both kinases, MKK4 and MKK7, VACV is not able to stimulate JNK1/2 phosphorylation. Therefore, this observation suggests a strict viral dependence on MKK4 and/or MKK7 to transmit downstream signals that lead to JNK1/2 phosphorylation. Regarding the individual contribution of MKK4 and MKK7 in VACV stimulation of JNK1/2, Fig. 1C (top) shows that in the absence of MKK4, MKK7 seems to be required to transmit signals to JNK1/2 upon VACV infection. Similarly, infections carried out in MKK7$^{-/-}$ cells (Fig. 1D, top) revealed that MKK4 seems to com-

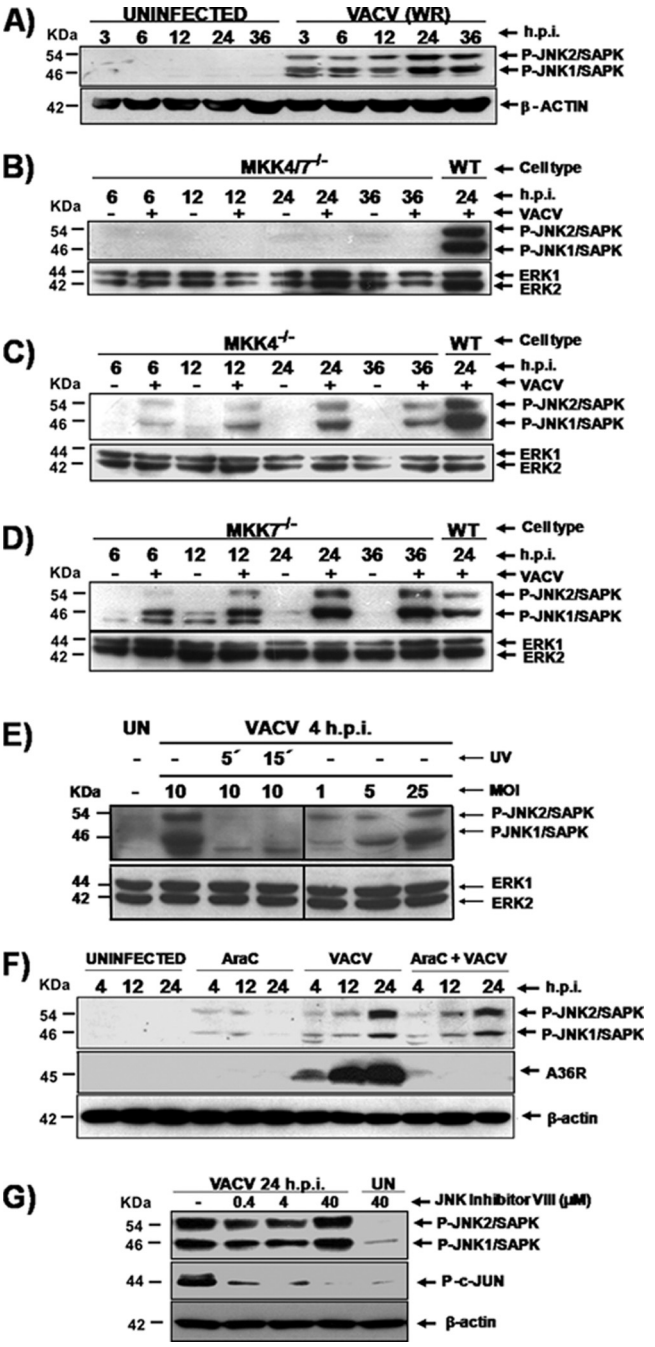

FIG 1 VACV activation of JNK1/2 requires either MKK4 or MKK7. VACV infections were carried out using mouse fibroblast A31 cells (A, E, and F), WT MEFs (B, C, D, and G), MKK4/7$^{-/-}$ MEFs (B), MKK4$^{-/-}$ MEFs (C), and MKK7$^{-/-}$ MEFs (D). Cells were either uninfected or infected (MOI, 10) for the times shown. Whole-cell extracts (WCEs) were collected and analyzed by Western blotting. (A to G) (Top) Immunoblots with anti-phospho JNK1/2/SAPK antibody; (bottom) immunoblot with anti-β-actin or total ERK12 as a loading control, as indicated. (F and G, middle) Immunoblots were also probed with antiviral A36R protein and anti-phospho-c-Jun antibodies, respectively. (E) Cells were infected with UV-inactivated virus (MOI, 10) or with the nonirradiated virus (MOI, 1, 5, or 25), as indicated. UN, uninfected. (F and G) Cells were incubated with araC (40 μg/ml) or with JNKi (0.4 to 40 μM) for 30 min prior to virus infection. Incubation was carried in the continued presence of the inhibitors. The molecular masses (kDa) are indicated on the left. Data are representative of three independent experiments with similar results.

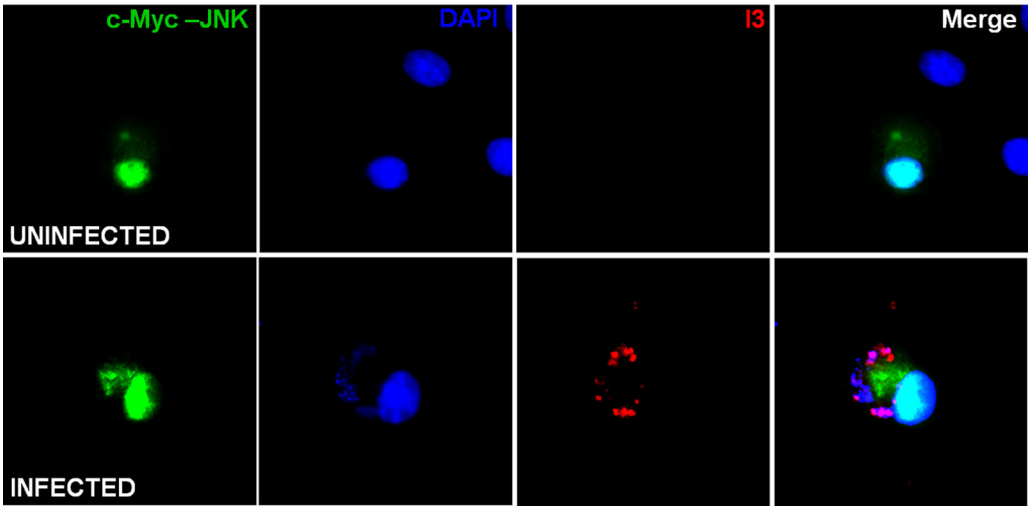

FIG 2 Phospho-JNK localization during VACV infection. BSC-40 cells were transfected with pcDNA3-cMyc-JNK2-MKK7 for 48 h, followed by infection with VACV for 7 h. At this time, cells were processed for fluorescence analyses and simultaneously stained with anti-c-Myc and antiviral protein I3 antibodies, followed by FITC-conjugated antimouse and rhodamine-conjugated antirabbit antibodies (green and red, respectively). To detect cellular and viral DNA, cells were stained with DAPI (blue).

pensate for the absence of MKK7 and stimulates JNK1/2 phosphorylation. Together, these data show that either MKK4 or MKK7 is individually able to transmit signals that result in JNK1/2 phosphorylation. Alternatively, VACV can stimulate both MKK4 and MKK7, most likely to maximize signaling to downstream molecules associated with diverse biological functions.

In order to address whether viral stimulation of JNK1/2 is dependent on early events during the viral replication cycle, the following experiments were designed. First, we investigated whether UV-inactivated virus was able to stimulate the kinases. Although UV irradiation renders the virus noninfectious, it does not affect viral DNA-dependent RNA polymerase activity, and transcription of the viral genome can occur following irradiation, even though it is not yet fully uncoated (17, 43). Thus, viruses were UV irradiated for 5 or 15 min, and A31 cells were exposed to the inactivated virions for 4 h. Whole-cell lysates were collected, subjected to Western blotting, and probed with the anti-phospho-JNK1/2 antibody. As shown in Fig. 1E, viral stimulation of JNK1/2 relies on events that take place after virus-receptor interaction. This reliance is evident by the fact that only the nonirradiated virus was able to stimulate phosphorylation of JNK1/2 by MKK4/7 at 4 hpi (Fig. 1E, second lane). In order to evaluate if viral stimulation of JNK1/2 is dependent on the MOI, a second experiment was designed. A31 cells were exposed to increasing MOIs, 1, 5, and 25, and the infection was allowed to proceed for 4 h. Whole-cell lysates were then collected, subjected to Western blotting, and probed as described above. As shown in the fifth to seventh lanes of Fig. 1E, JNK1/2 phosphorylation occurs with the various MOIs, thus demonstrating that this phenomenon is a virus-specific and MOI-dependent event.

To investigate whether the sustained JNK1/2 stimulation in the later phase of the infectious cycle was dependent on events taking place after viral DNA replication, A31 cells were infected with VACV at an MOI of 10 either in the presence or in the absence of araC (40 μg/ml), an inhibitor of viral DNA replication. Cells were harvested at 4, 12, and 24 h and whole-cell lysates were collected and immunoblotted with anti-phospho-JNK1/2 (upper) or anti-viral A36R (middle) antibodies. As shown in Fig. 1F, while inhibition of viral DNA replication appears to slightly reduce JNK1/2 phosphorylation, it did abolish A36R expression. Altogether, these findings revealed that JNK1/2 stimulation does require the expression of viral early genes but does not necessarily require intermediate or late gene expression.

To rule out the possibility that any alterations may have occurred during the generation of KO cells, a complementary approach was designed. We investigated the effect of the pharmacological inhibitor JNK inhibitor VIII (JNKi), an ATP-competitive reversible inhibitor of JNK which inhibits c-Jun phosphorylation, a classical substrate of this kinase (2, 35). In order to show the functionality of this JNKi in our cells, WT MEFs were infected with VACV at an MOI of 10 either in the absence or in the presence of various concentrations of JNKi (0.4 to 40 μM), as indicated in Fig. 1G. Cells were incubated for 24 h, and then whole-cell lysates were collected and immunoblotted with anti-phospho-JNK1/2 (Fig. 1G, top) or anti-phospho-c-Jun (Fig. 1G, middle) antibodies. As shown in Fig. 1G, viral activation of c-Jun was greatly affected when the infection was carried out in the constant presence of JNKi (second to fourth lanes).

Phospho-JNK is relocalized during VACV infection. In light of the fact that JNK1/2 are phosphorylated throughout VACV infection, we decided to monitor phospho-JNK2 localization in the infected cell. To this end, BSC-40 cells were transfected with pcDNA3-cMyc-JNK2-MKK7 to allow the transient expression of this fusion protein, in which JNK2 is constitutively active. At 48 h posttransfection, cells were infected with VACV and processed for immunofluorescence at 7 hpi, as shown in Fig. 2, whereas the majority of phospho-JNK2 distributed exclusively in the nucleus of uninfected cells (top, green); during infection, the kinase is distributed in the nucleus as well as in the cytoplasm, where infection takes place (bottom, green). The viral factories can be visualized in the cytoplasm by the positive staining of both viral single-strand binding protein I3 and DNA (bottom, red and blue, respectively). These results demonstrate that JNK is relocalized during VACV infection, and its redistribution in both the nucleus

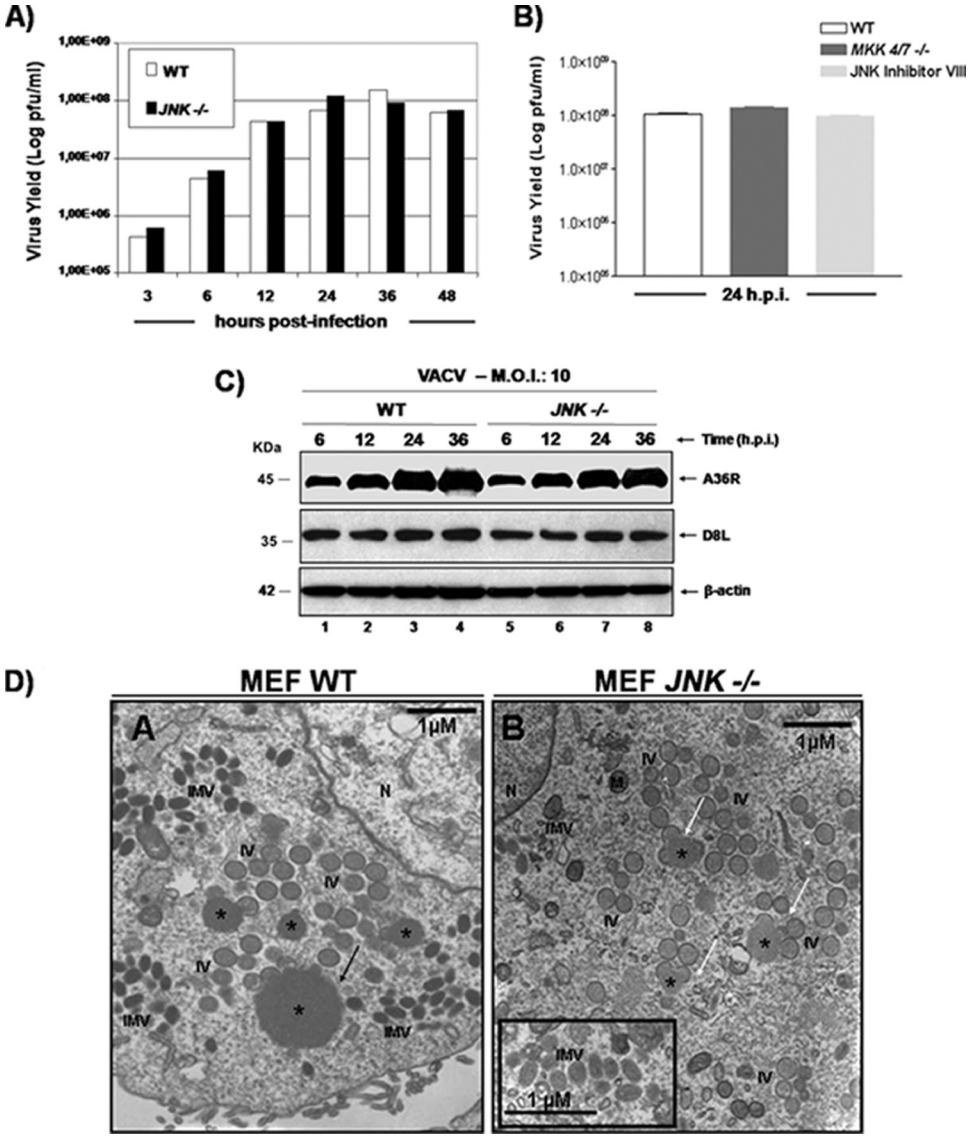

FIG 3 The VACV-stimulated MKK4/7-JNK1/2 pathway is not required for virus replication. (A) Growth curve of VACV performed in WT and JNK1/2-KO MEFs. Cells were infected with VACV at an MOI of 10 and harvested at 3, 6, 12, 24, 36, or 48 hpi, and viral yield was quantitated by viral plaque assay. Data are representative of at least three independent experiments. (B) WT MEFs were incubated in either the absence or presence of JNKi (4 μM) for 30 min. WT and MKK4/7-KO cells were infected (MOI, 10) with VACV for 24 h and assayed for viral production. Data are means of triplicate experiments + SDs. (C) WT or JNK1/2$^{-/-}$ MEFs were infected (MOI, 10) with VACV for the times shown, and 40 μg of WCEs was subjected to Western blotting. (Top and middle) Immunoblots with anti-A36R or anti-D8L antibodies; (bottom) anti-β-actin antibody was used as a loading control. The molecular masses (kDa) are indicated on the left. Data are representative of three independent experiments with similar results. (D) Confluent monolayers of WT and JNK1/2$^{-/-}$ MEFs were serum starved for 12 h and then infected with VACV at an MOI of 2 for 18 h. Cells were fixed and prepared for transmission electron microscopy. Micrographs are shown with their scale indicated by the bars. WT and JNK1/2$^{-/-}$ MEFs contain all the normal intermediates in virion morphogenesis (A and B). (B, inset) Detail highlighting the IMV form. Abbreviations: *, virosomes; IV, immature virions; IMV, intracellular mature virions; M, mitochondria; N, nucleus.

and cytoplasm might suggest a role for this kinase during the virus life cycle.

The VACV-stimulated MKK4/7-JNK1/2 pathway is not required for viral replication. To investigate whether the MKK4/7-JNK1/2 pathway played a relevant role in viral growth, we infected WT and JNK1/2-KO cells with VACV at an MOI of 10. At 3, 6, 12, 24, 36, and 48 hpi, virus was collected and assayed for viral yield. As shown in Fig. 3A, the absence of JNK1/2 does not affect VACV replication since the IMV yield measured in the JNK1/2-KO cells paralleled that measured in WT cells. We also investigated the upstream regulators of JNK1/2, MKK4/7. For that, MKK4/7-KO cells were infected with VACV (MOI, 10), and at 24 hpi, the viral yield was determined. Figure 3B shows the viral yields obtained from triplicate cultures. Consistent with the data generated with the JNK-KO cells (Fig. 3A), virus replication was not affected by the double mutation MKK4/7$^{-/-}$, demonstrating that the MKK4/7-JNK1/2 pathway is not associated with virus replication (Fig. 3B). In line with these observations, treatment of WT cells with JNKi also did not have an effect on viral multiplication (Fig. 3B, light gray bar). These findings were also corroborated by the data

shown in Fig. 3C, where expression of the viral late genes A36R and D8L was investigated. WT and JNK1/2-KO cells were infected with VACV (MOI, 10) for 6, 12, 24, and 36 h. At each time, whole-cell lysates were immunoblotted with antiviral D8L or A36R antibodies. As demonstrated in Fig. 3C (top and middle), the absence of JNK1/2 did not appear to change viral late gene expression, since A36 and D8 proteins were detected to the same extent in both KO and WT cell lines. Finally, electron microscopy analysis of WT and KO cells showed the full spectrum of intermediate virions, including crescents, immature virions (IVs), intracellular mature virions (IMVs), and enveloped virions (EVs; EEVs or CEVs; data not shown), which are typically seen in virion morphogenesis. All of these stages of morphogenesis were observed not only in the WT cells (Fig. 3D, panel A) but also in JNK1/2-KO cells (Fig. 3D, panel B). However, in JNK1/2-KO MEFs (Fig. 3D, panel B, white arrow), we consistently observed that virosomes (large viroplasm subdomains within the surrounding viral factory surrounded by arch-shaped crescent structures [7]) did not achieve sizes equal to those of virosomes in WT cells (Fig. 3D, panel A, black arrow). In order to quantify this phenomenon, we measured the diameter of virosomes in infected WT and KO cells (30 cells were counted). While the average size of WT cell virosomes was 860.22 nm, we found that the KO cell virosome measured was 484.64 nm. Of note, in WT cells the largest virosome found was 2,692.58 nm, while the one in KO cells was 1,201.47 nm. On the other hand, the smallest virosome found in WT cells was 312.69 nm, and the smallest virosome found in KO cells was 269.53 nm (data not shown). Furthermore, while the same virion intermediates found to be present during morphogenesis were frequently grouped together at specific locations of the cytoplasm in WT cells, these intermediates were more frequently dispersed in the KO cells (Fig. 3D, panel B).

VACV-infected JNK1/2$^{-/-}$ MEFs exhibit reduced early cell contractility. It has been known that during the course of VACV infection both MT and actin networks undergo accentuated modifications that facilitate the inward and outward movement of viral particles (21, 24, 26, 27, 28, 38). To investigate whether JNK is associated with cytoskeleton alterations that follow VACV infection, WT and JNK1/2-KO cells were either uninfected or infected with VACV (MOI, 5). At 3, 6, and 12 hpi, cells were fixed and stained with anti-β-tubulin (green) or with rhodamine-conjugated phalloidin (red), and the images were visualized by confocal microscopy. In uninfected WT cells, MTs are present at the cell surface and at the perinuclear MT-organizing center (MTOC) toward the plasma membrane (Fig. 4a). Under the same conditions, the actin filament (AF) staining revealed numerous stress fibers at the cell surface (Fig. 4b, inset). The merged image shows that both AFs and MTs reached the cell periphery (Fig. 4c, inset). In contrast, uninfected JNK1/2-KO cells had multiple projections presenting a distinct cell shape (Fig. 4m to o). In spite of this, cortical stress fibers were still present (Fig. 4n, inset) and peripheral actin and MTs colocalized at the cell periphery (Fig. 4o, inset).

Upon VACV infection, the cells underwent diverse morphological changes (to distinct morphotypes, which are associated with the cytopathic effect [CPE]), and their predominant phenotypes were categorized morphotypes 1 through 7 (Fig. 4f, i, l, r, u, and x and 5A). Of note, the predominant morphotypes observed in the WT (morphotypes 1 to 3) and KO (morphotypes 4 to 7) cells are described as follows. In morphotype 1, the early phase of infection (3 hpi) in WT MEFs was characterized by cell shrinkage and loss of cell-to-cell contacts, while MTs retracted from the cell periphery and concentrated in loops at the perinuclear area. Actin remained at the cell periphery (Fig. 4f, inset), but stress fibers were drastically reduced (Fig. 4f and e, insets). These data are consistent with previous observations (21, 26, 27, 28), and morphotype 1 predominated at between 3 and 6 hpi (Fig. 4, graph 1) and at those times represented about 70 and 55% of the cells, respectively. By 6 hpi, morphotype 2 was detected, with WT cells again being flattened and MTs protruding from the center toward the cell periphery (Fig. 4g and insets in Fig. 4i). Stress fibers were present throughout the cell, highlighting the cortical actin, and actin tails became more frequent (Fig. 4h, dashed arrows). By 6 hpi, morphotypes 1 and 2 were the most abundant (Fig. 4, graph 2), representing about 55 and 40% of the cells, respectively. By 12 hpi, morphotype 3 was identified, with WT cells becoming multibranched, reminiscent of neurite-like projections that consist of microtubule bundles (Fig. 4j [arrows] and l [inset]) (21, 26). There was no obvious formation of stress fibers, and at this time morphotypes 2 and 3 predominated, corresponding to 30 and 40% of the cells, respectively (Fig. 4k, inset, and Fig. 4, graph 3). In contrast, in the absence of JNK1/2, these virus-induced changes in cell morphology were largely affected. After 3 hpi, cells displayed morphotype 4, which was very similar to the morphotype of uninfected JNK-KO cells, even though stress fibers appeared to be less organized and diffused (Fig. 4q [inset] and r). Morphotype 4 was the most predominant morphology at 3 and 6 hpi and represented about 60 and 70% of the cells, respectively (Fig. 4, graph 4). Although JNK1/2 deletion greatly impaired early cell contractility, we observed that 38 and 25% of KO MEFs had a rounded morphotype 1 morphology at 3 and 6 hpi, respectively. Of note, morphotype 2 was barely found in the KO cells (Fig. 4, graph 2).

By 12 hpi, the multibranched morphotypes 5 and 6 were well represented, and both corresponded to close to 45% of infected KO cells (Fig. 4s to u and v to x, respectively, and graphs 5 and 6, respectively). In morphotype 5, the stress fibers, though less organized, were still visualized (Fig. 4t, inset), as were some actin tails (Fig. 4t, dashed arrows). In contrast, morphotype 6 was represented in cells that were more contracted and presented large MT protrusions that reached the cell periphery (Fig. 4v [arrows] and x [inset]). Nonetheless, there was no obvious stress fiber formation (Fig. 4w, inset). In about 35% of infected JNK-KO cells, morphotype 3 was also clearly identified (Fig. 4, graph 3).

VACV-infected JNK1/2$^{-/-}$ MEFs exhibit reduced cell motility. During the VACV infectious cycle, infected cells undergo migration, a process that not only is dependent on the virus-cell ligand interaction but that also requires expression of viral early genes (26, 27, 28) and repression of RhoA signaling by the viral protein F11L (34). During our analysis of VACV-induced cytopathic effects, typical migrating cells were observed in both WT and KO cells. A representative WT cell of the migrating phenotype (morphotype 7) is shown in Fig. 5A (panels a to c), with its relative abundance presented below. An actin-rich region was found at the leading edge of the cellular protrusion (Fig. 5A, panel b, bracket). This region comprised actin bundles organized into filopodia and a dense actin network forming a ruffling lamellipodium, which promotes forward movement, whereas MTs radiated from the MTOC (Fig. 5A, panel a). At the trailing edge and at the cell body, filamentous actin was shown representing stress fibers, which are

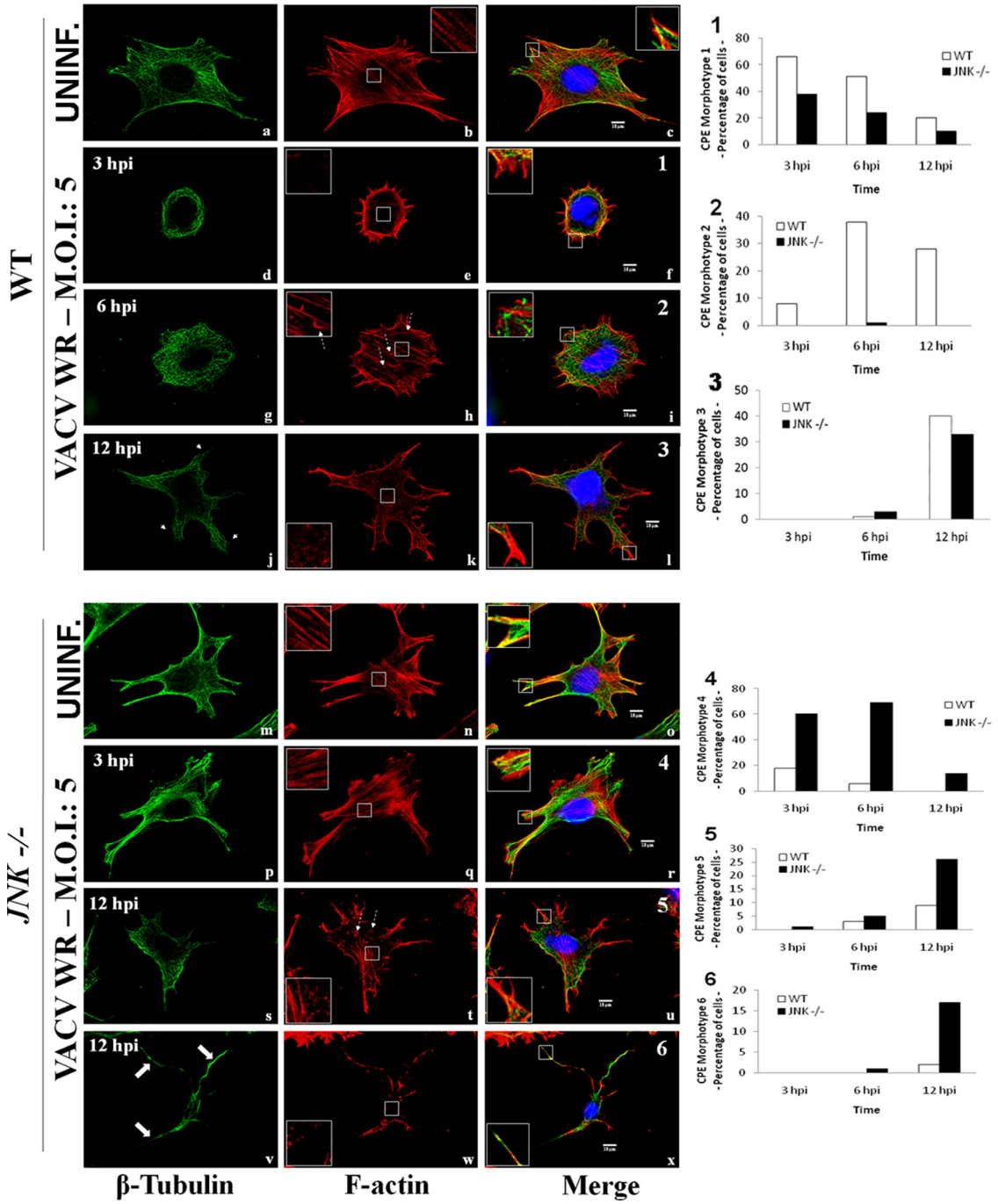

FIG 4 VACV-infected JNK1/2$^{-/-}$ MEFS exhibit reduced early cell contractility. WT (a to l) and JNK1/2-KO (m to x) MEFs were infected with VACV WR (MOI, 5). At 3, 6, or 12 hpi, cells were fixed and stained for the microtubule and actin networks. β-Tubulin, F-actin, and the nucleus are stained with FITC-conjugated antimouse secondary antibody (green), rhodamine conjugated-phalloidin (red), and DAPI (blue), respectively. Fluorescently labeled cells were visualized using a Zeiss (LSM 510 META) confocal microscope. The graphic representations of the relative abundance of each phenotype found in WT-infected cells (graphs 1 to 3, f, i, and l) or JNK1/2$^{-/-}$-infected cells (graphs 4 to 6, r, u, and x) are shown on the right ($n > 100$). (Left column) Thin arrows, microtubule projections (j); large arrows, microtubule long protrusions (v); (middle column) insets, cortical F-actin in detail, highlighting the presence (b, h, n, q, and t) or absence (e, k, and w) of stress fibers; dashed arrows, actin tails (h and t); (right column) insets, the edge of cell protrusions in detail, highlighting the protraction (c, i, l, o, r, u, and x) or retraction (f) of microtubule. Insets represent enlargement of the area indicated by the white box in the panel.

associated with the contraction of the cell body and retraction of the trailing edge (Fig. 5A, panel b, arrow) (10).

Because morphotype 7 was less frequent in JNK1/2-KO cells, as seen in the graph in Fig. 5A, and since it has been shown that JNK can be required for cell migration, we wondered whether these virus-stimulated kinases are implicated in VACV-stimulated cell motility (13). To address this question, wounds were made in WT MEFs and JNK1/2-KO and MKK4/7-KO confluent cell monolay-

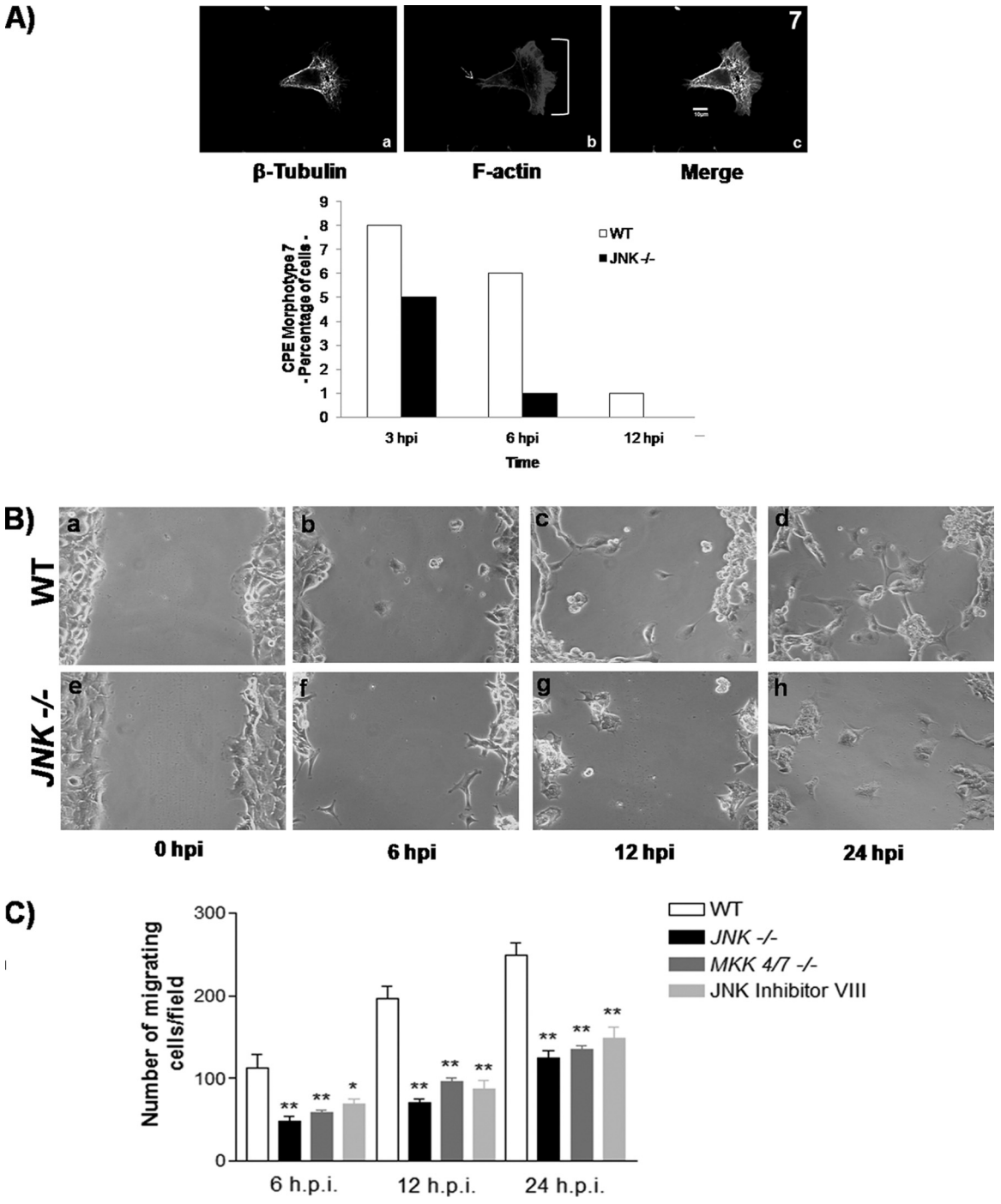

FIG 5 VACV-infected JNK1/2$^{-/-}$ MEFs exhibit reduced cell motility. (A) WT and JNK1/2-KO MEFs were infected with VACV at an MOI of 5 for 3, 6, or 12 h. Cells were then fixed, permeabilized, blocked, and stained with mouse anti-β-tubulin, followed by FITC-conjugated antimouse secondary antibody and rhodamine-conjugated phalloidin. (Panels a to c) Representative image of the migratory morphotype 7; (panel b) arrow, the trailing edge; bracket, the lamellipodia. The graphic representation of the relative abundance of this phenotype in WT or JNK1/2$^{-/-}$ VACV-infected cells is shown at the bottom of panel A ($n > 100$). (B) Phase-contrast images of scratched confluent monolayers of WT or JNK1/2$^{-/-}$ MEFs infected with VACV (MOI, 5). Cells were fixed at 0, 6, 12, and 24 hpi and processed for microscopic analysis. (C) Graphic representations of the number of migrating cells per 5 mm in the wounded area of confluent monolayers of WT, JNK1/2$^{-/-}$, or MKK4/7$^{-/-}$ MEFs as well as WT cells treated with JNKi (4 μM) and then infected with VACV at an MOI of 5. *, $P < 0.01$; **, $P < 0.001$; $n = 10$ fields counted.

ers. WT MEFs were incubated in either the absence or presence of JNKi (4 μM) for 30 min prior to virus infection. These cells were then infected with VACV (MOI, 5), and the migration of infected cells into the wounded area was observed at 6, 12, and 24 hpi. Our findings (Fig. 5B and C) revealed that virus-induced cell migration was reduced at all time points both in JNK1/2-KO and MKK4/7-KO cells and in the WT MEFs pretreated with JNKi (only the data from experiments carried out with JNK1/2-KO cells are

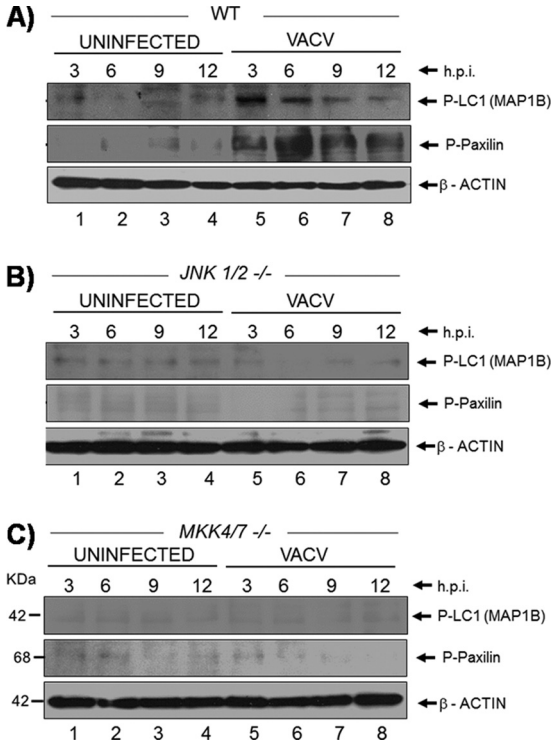

FIG 6 Absence of JNK affects the phosphorylation of both microtubule-associated protein (MAP-1B) and paxillin. (A to C) WT, JNK1/2-KO, and MKK4/7-KO cells were left uninfected or infected (MOI, 5). At 3, 6, 9, and 12 hpi, cell lysates were collected, subjected to Western blotting, and then probed with anti-phospho-MAP-1B (top) or anti-phospho-paxillin (middle) antibodies. (Bottom) Probing with anti-β-actin antibody as a loading control. The molecular masses (kDa) are indicated on the left. Data are representative of three independent experiments with similar results.

shown [Fig. 5B, panels e to h]) compared to the WT cells (panels a to d). In order to quantify these findings, the numbers of migrating cells per field at each time point postinfection were counted ($n > 100$), and the results are shown in Fig. 5C. Our data indicate a reduction of $\geq$50% in virus-induced cell motility in both JNK1/2-KO and MKK4/7-KO cells. Interestingly, the same level of inhibition was observed for JNKi, thus uncovering an important role for the MKK4/7-JNK1/2 pathway in virus-induced cell motility.

Phosphorylation of microtubule-associated protein (MAP-1B) and paxillin is affected in infected JNK1/2-KO cells. Considering that the absence of JNK altered both the cytoskeleton organization (Fig. 4) and the migration of infected JNK1/2-KO cells (Fig. 5) and on the basis of the fact that MAP-1B and paxillin proteins are both downstream targets of JNK (2), we wondered whether these substrates were affected in the infected JNK-KO cells compared to WT cells. To approach that, WT MEFs and JNK1/2-KO and MKK4/7-KO cells were infected (MOI, 5) for 3, 6, 9, and 12 h. The whole-cell lysates were collected, subjected to Western blotting, and probed with anti-phospho-MAP-1B and -paxillin antibodies. Our findings revealed that while both MAP-1B and paxillin proteins were phosphorylated upon VACV infection in the WT cells (Fig. 6A, top and middle), no phosphorylation was verified in either JNK1/2-KO or MKK4/7-KO cells (Fig. 6B and C).

Viral trafficking to the cell periphery, EEV release, and virus plaque size are affected in JNK1/2-KO cells. Since VACV trafficking to the cell periphery is dependent on the MT network and we showed that infected JNK1/2-KO cells have a pronounced alteration in MT dynamics (Fig. 4), we hypothesized whether, under this circumstance, viral trafficking could be affected (24, 38). To address this question, WT and JNK1/2-KO cells were infected with VACV vF13L-GFP (MOI, 5) for 9 h. Cells were fixed and blocked without permeabilization in order to avoid antibody internalization, a condition that allows us to detect only the cell-associated enveloped virus (CEV) by using the antiviral B5 antibody. Results for a single WT or KO cell ($n > 100$) are shown in Fig. 7A. As observed, viral particles are reaching the cell periphery, though there was an increase in CEV detected at the surface of the JNK1/2-KO cell compared to the WT cell (Fig. 7A, panels e and f, white arrows).

Given that CEV accumulation at the surface of JNK1/2-KO MEFs may be due to enhanced IEV trafficking and/or defective viral detachment, we decided to examine if the release of enveloped particles was affected. To approach this question, WT or JNK1/2-KO MEFs were seeded and counted before infection to make sure that the same numbers of cells were infected. Supernatants from WT or JNK1/2-KO MEFs infected with VACV at an MOI of 10 for 48 h were then collected, centrifuged, and incubated with anti-IMV monoclonal antibody L1R in order to neutralize any IMV particles remaining in the supernatant (42). EEVs obtained from both cell lines were then titrated. As shown in Fig. 7B, JNK1/2-KO cells had an increase in EEV release of about 75% compared to WT cells. To further clarify this phenomenon, we investigated the size of the viral plaque formed in the absence of JNK1/2. WT and JNK1/2-KO cells were infected with VACV for 72 h in liquid or in agarose-supplemented solid medium. On the basis of the data presented in Fig. 7C, we concluded that the size of the viral plaques was also enhanced in the absence of JNK1/2. Therefore, this increase in the viral plaque size supports a role for the MKK4/7-JNK1/2 pathway in the regulation of trafficking and egress of enveloped VACV from infected cells. Indeed, comet-like plaques were also observed in JNK1/2-KO cells, corroborating the increase in the release of EEV (Fig. 7C, liquid medium).

DISCUSSION

It is becoming increasingly apparent that the intracellular environment plays a vital role in orthopoxvirus biology (3, 19). We have previously shown that during the early phase of the VACV infectious cycle both MEK/ERK and PI3K/Akt pathways are stimulated. In fact, this stimulation has been shown to be a benefit for the virus infection, since its genetic or pharmacological blockade results in decreased viral replication (1, 9, 29, 30).

In this report, we present evidence that VACV stimulates JNK1/2 in a sustained manner during the entire infectious cycle from 3 to 36 hpi and that such stimulation plays an important role in the dissemination of enveloped virus, CEV. Genetic approaches allowed us to firmly establish the MKK4/7-JNK1/2 pathway to be a virus-regulated signal transduction pathway, which was corroborated by the fact that only nonirradiated VACV was able to stimulate the pathway. The earliest activation of JNK1/2 upon VACV infection was observed at 1 hpi (data not shown), which implies that an early event subsequent to interaction with the virus receptor is required. Moreover, postreplication events are not required for JNK1/2 phosphorylation (Fig. 1F). Taken together, these data

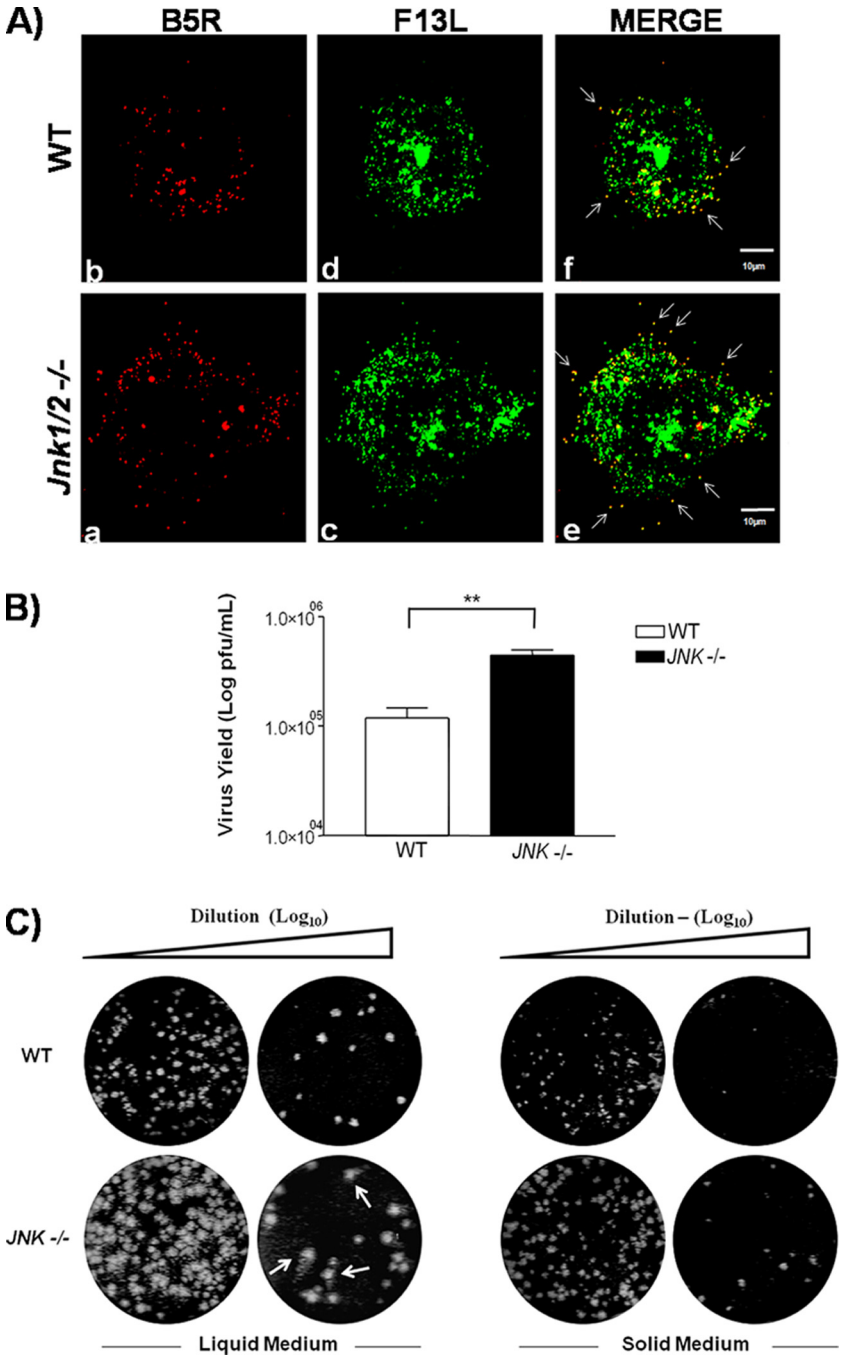

FIG 7 Viral trafficking to the cell periphery is deregulated in JNK1/2-KO cells. (A) Detection of CEV in the cell surface by confocal microscopy. WT and JNK1/2-KO MEFs were infected with VACV vF13L-GFP at an MOI of 5 for 9 h. Cells were fixed and blocked without permeabilization and then incubated with mouse anti-B5 antibody, followed by staining with rhodamine-conjugated antimouse secondary antibody. White arrows indicate CEVs. Micrographs are shown with their scales indicated by the bars. (B) Absence of JNK1/2 affects the release of EEV from the infected cells. Culture supernatants of VACV-infected WT and JNK1/2/KO cells at an MOI of 10 for 48 h were incubated with the anti-IMV-specific L1R antibody (1:1,000) at 37°C for 1 h and then titrated in BSC-40 cells. Data are representative of at least three independent experiments with similar results (**, $P < 0.05$). (C) Viral plaque size is increased in the KO cells. WT and JNK1/2-KO MEFs were infected with serial dilutions of VACV in liquid or agarose-supplemented (solid) medium. At 72 hpi, cells were fixed and stained with crystal violet. Comet-like plaques (arrows) were visualized in the KO cells.

strongly suggest that only early events in the viral life cycle are necessary to activate JNK1/2.

Furthermore, our results revealed that JNK1/2 kinases not only are phosphorylated during infection but also are recruited from the nucleus to the cytoplasm (Fig. 2), where viral replication takes place. However, even though the time frame of the virally stimulated MKK4/7-JNK1/2 pathway covers the entire viral replication cycle, including morphogenesis, assembly, and release of infec-

tious particles, we were able to verify that deletion of JNK1/2 does not affect the generation of IMV using three different approaches: electron microscopy, viral late gene expression, and viral growth curve (Fig. 3). Even though all stages of viral morphogenesis were observed in both WT and KO cell lines, we also noticed that virosomes in the KO cells do not achieve the same size as those in WT cells (Fig. 3C and data not shown).

These observations, however, are in apparent contrast to those of Hu and colleagues (12). These authors have shown that by separately infecting either JNK1 or JNK2-KO cells with VACV WR to quantitate viral titers, a 40-fold increase was observed with JNK1-KO cells, which was paralleled by the infection of JNK2-KO cells, though to a lesser extent than for the WT cells. They also correlated the enhanced viral replication with enhanced cell death and virus-induced apoptosis. In fact, it has been demonstrated that JNK1 and JNK2 are responsible for the phosphorylation of Bid, which is a proapoptotic BH3-only member of the Bcl2 group, and that JNK1/2-KO cells are resistant to apoptosis mediated via the intrinsic pathway (32). In our hands, the experiments were carried out in JNK1/2-double-KO cells, and while we did not notice a significant increase in the viral yield or any signs of cell death during infection, we decided to monitor whether cells underwent apoptosis. Indeed, we were not able to find any evidence of apoptotic cell death in VACV-infected JNK1/2-KO cells on the basis of activation of the executioner caspase-3 or its substrate, poly(ADP-ribose) polymerase (data not shown). On the contrary, the data presented by the authors mentioned above (12) did not exclude the possibility that infection of either JNK1-KO cells (which still express JNK2) or JNK2-KO cells (which still express JNK1) is enough to stimulate the apoptotic pathway. It is conceivable that the presence of one of the isoforms in the single-KO cells could, in turn, account for the enhanced cell death associated with the enhanced virus replication. It is possible that the costimulation of both JNK1 and JNK2 and not just one of the isoforms during the viral life cycle could be of relevance to VACV biology.

In addition, we also provided evidence that VACV replication was not affected by the absence of both MKK4/7 proteins, the well-known upstream regulators of JNK1/2. Moreover, the pharmacological inhibitor of JNK, JNK inhibitor VIII (JNKi), also had no effect on infected WT cells. As demonstrated in Fig. 3B, none of them showed reduced viral production.

Furthermore, our data present evidence that infection of WT cells with VACV is accompanied by the disruption of both MT and actin networks (Fig. 4a to l) and are in agreement with data reported by others (21, 27, 28). These virus-induced alterations, however, were less pronounced in the JNK1/2-KO cells (Fig. 4a to l and m to x). Remarkably, the most pronounced effect of the VACV-stimulated MKK/JNK pathway seemed to be the transition from the rounded morphotype 1 to the flattened morphotype 2 (Fig. 4, graphs 1 and 2). While morphotype 1 was found in the KO cells at reasonable amounts (38 and 25% at 3 and 6 hpi, respectively), morphotype 2 was barely found in these cells. Thus, the VACV-stimulated MKK4/7-JNK1/2 pathway appears to play a significant role in the virus-induced alterations at the cytoskeleton architectures. These alterations are required for the progress of the cytopathic effect as the infection evolves. This assumption was further corroborated by the finding that phosphorylation of the microtubule-associated protein MAP-1B, which has been shown not only to stabilize MT but also to bind actin filaments (13, 31), was not detected in the JNK-KO cells (Fig. 6). Moreover, the kinetics of MAP-1B phosphorylation, which peaked at 3 to 6 hpi (Fig. 6), coincided with the time frame required for the transition from morphotype 1 to morphotype 2 (Fig. 4d to f and g to i and graph 2).

It is worth noting that virus stimulation of the MKK4/7-JNK1/2 pathway is required for cell migration. In agreement with the viral need for early gene expression to stimulate cell migration (26, 27, 28), we provided evidence that this event was significantly affected in the MKK/JNK-KO cells (Fig. 5B and C). Consistent with the requirement of paxillin phosphorylation (PX-P) for cell migration as well (13, 14), upon infection, PX-P was detected only in the WT cells (Fig. 6).

Our data also show that the IMV assembly is not impaired in KO cells (Fig. 3D), but on the other side, trafficking of the virus to the cell periphery is altered in those cells as a consequence of changes in the dynamics of MT networks (Fig. 4 and 7). These findings appear to be distinct from the data reported by Ploubidou et al. (21), who have shown that the administration of nocodazole, a microtubule-depolymerizing drug, strictly affected enveloped virion morphogenesis but not IMV formation. Taking this into consideration, the total disorder of the MT network caused by nocodazole during VAC infection observed by Ploubidou et al. (21) is not similar to that identified in our infected JNK1/2-KO cells, where the MT arrangement is still visualized as a network; however, it is much less organized at 3 to 6 hpi. In addition, Schepis et al. (27) demonstrated that VACV infection requires intact MTs to rearrange the actin network, which occurs in parallel with the changes in cell shapes during each step of the virus cycle. However, the mechanism by which VACV rearranges MT and actin networks through the MKK/JNK pathway requires further studies.

Therefore, the observation that the MKK4/7-JNK1/2 pathway does not play a relevant role in VACV IMV formation (Fig. 3), though its activation occurred even at late times during the infection (>12 hpi), favors the hypothesis that viral stimulation of the pathway may have implications for VACV biology other than viral production. In fact, our data are consistent with a regulatory role exerted by this pathway on normal egress of CEV from infected cells and EEV release (Fig. 7A and B). In addition, studies of Schramm and coworkers (28) suggest that VACV-induced cell contractility might downregulate protein and viral particle trafficking to the cell membrane during the early phase of the infectious cycle, thereby functioning as an immune evasion mechanism. Thus, we hypothesize that since JNK1/2 can regulate traffic to the cell membrane and/or exocytosis of cellular proteins, the same mechanism could coordinate EEV release, enabling VACV to control viral antigen exposure and, therefore, the level of host immune response.

A schematic representation of our model regarding the VACV-stimulated MKK4/7-JNK1/2 pathway and its biological consequences is depicted in Fig. 8. After IMV penetration and primary uncoating, replication-competent virus and expression of viral early genes only seem to be required to stimulate the pathway (Fig. 8, steps 1 and 2). Although the activation of this pathway is not necessary for the production of IMV particles, it does play a regulatory role in the virus-stimulated cell contractility/morphology and cell migration, which appears to be associated with the activation of microtubule-associated protein 1B and paxillin proteins, respectively (Fig. 8, step 3). Altered microtubule and actin networks in the absence of JNK1/2 are associated with deregulated

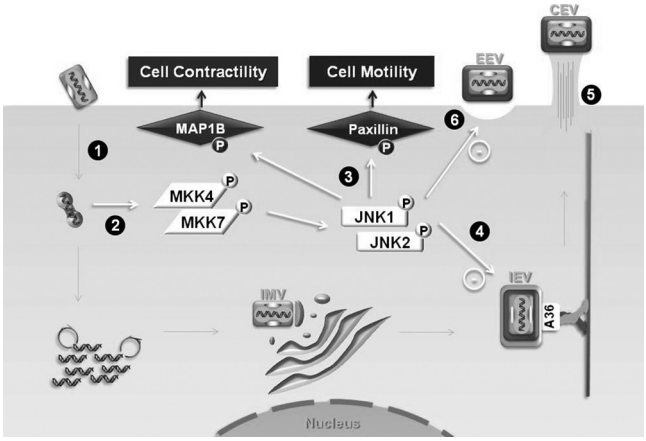

FIG 8 Schematic representation of the VACV-stimulated MKK4/7-JNK1/2 pathway and its biological consequences. Soon after IMV penetration and uncoating (step 1), replication-competent virus is required for the stimulation of the MKK4/7-JNK1/2 pathway (step 2). The pathway does play a relevant role in virus-stimulated cell migration and cell contractility/morphology (step 3), although it does not affect viral productivity. IEV is then formed and transported to the cell periphery (step 4). Altered microtubule and actin cytoskeleton organization in the JNK-KO cells is followed by deregulated accumulation/release of viral enveloped form, i.e., increased accumulation of CEV (step 5) at the surface as well as release of EEVs (step 6).

viral trafficking to the periphery and enhanced EEV release (Fig. 8, steps 4 to 6).

ACKNOWLEDGMENTS

We are grateful to Angela S. Lopes, Ilda M. V. Gama, João R. dos Santos, and Andreza A. Carvalho for their secretarial/technical assistance and to Fernanda Gambogi for help with immunofluorescence microscopy. We also thank M. C. Sogayar (Department of Biochemistry, University of São Paulo, São Paulo, Brazil), who kindly provided us with the A31 cell line, and R. Davis (Howard Hughes Medical Institute, University of Massachusetts Medical School, Worcester, MA) for the WT and JNK1/2-, MKK4-, MKK7-, and MKK4/7-KO cells. VACV WR was from C. Jungwirth (Universität Würzburg, Würzburg, Germany). The recombinant VACV vF13L-GFP and the rabbit polyclonal antibodies against viral proteins, B5R, D8L, L1R, and A36R, were from B. Moss (NIAID, Bethesda, MD). The pcDNA3-Myc-JNK2-MKK7 WT plasmid was from Eugen Kerkhoff (Universität Würzburg, Würzburg, Germany). We also thank Flávio G. da Fonseca (UFMG, Belo Horizonte, MG, Brazil) and Kathleen A. Boyle (Medical College of Wisconsin, Milwaukee, WI) for critically reading the manuscript.

This work was supported by grants from Fundação de Amparo a Pesquisa do Estado de Minas Gerais (FAPEMIG), the Brazilian Federal Agency for Support and Evaluation of Graduate Education (CAPES), and the National Council for Scientific and Technological Development (CNPq). A.C.T.C.P., B.S.A.F.B., F.G.G.L., and J.A.P.S.-M. were recipients of predoctoral fellowships from CNPq. C.A.B., E.G.K., T.S.-P., P.F.P.P., and P.C.P.F. are recipients of research fellowships from CNPq.

REFERENCES

1. **Andrade AA, et al.** 2004. The vaccinia virus-stimulated mitogen-activated protein kinase (MAPK) pathway is required for virus multiplication. Biochem. J. **381**:437–446.
2. **Bogoyevitch MA, Kobe B.** 2006. Uses for JNK: the many and varied substrates of the c-Jun N-terminal kinases. Microbiol. Mol. Biol. Rev. **70**:1061–1095.
3. **Bonjardim CA, Ferreira PC, Kroon EG.** 2009. Interferons: signaling, antiviral and viral evasion. Immunol. Lett. **122**:1–11.
4. **Campos MAS, Kroon EG.** 1993. Critical period for irreversible block of vaccinia virus replication. Rev. Microbiol. **24**:104–110.
5. **Chang L, Jones Y, Ellisman MH, Goldstein LS, Karin M.** 2003. JNK1 is required for maintenance of neuronal microtubules and controls phosphorylation of microtubule-associated proteins. Dev. Cell **4**:521–533.
6. **Chang L, Karin M.** 2001. Mammalian MAP kinase signalling cascades. Nature **410**:37–40.
7. **Condit RC, Moussatche N, Traktman P.** 2006. In a nutshell: structure and assembly of the vaccinia virion. Adv. Virus Res. **66**:31–124.
8. **Davis RJ.** 2000. Signal transduction by the JNK group of MAP kinases. Cell **103**:239–252.
9. **de Magalhaes JC, et al.** 2001. A mitogenic signal triggered at an early stage of vaccinia virus infection: implication of MEK/ERK and protein kinase A in virus multiplication. J. Biol. Chem. **276**:38353–38360.
10. **Etienne-Manneville S.** 2004. Actin and microtubules in cell motility: which one is in control? Traffic **5**:470–477.
11. **Hollinshead M, et al.** 2001. Vaccinia virus utilizes microtubules for movement to the cell surface. J. Cell Biol. **154**:389–402.
12. **Hu W, et al.** 2008. JNK-deficiency enhanced oncolytic vaccinia virus replication and blocked activation of double-stranded RNA-dependent protein kinase. Cancer Gene Ther. **15**:616–624.
13. **Huang C, Jacobson K, Schaller MD.** 2004. MAP kinases and cell migration. J. Cell Sci. **117**:4619–4628.
14. **Huang C, Rajfur Z, Borchers C, Schaller MD, Jacobson K.** 2003. JNK phosphorylates paxillin and regulates cell migration. Nature **424**:219–223.
15. **Husain M, Moss B.** 2003. Intracellular trafficking of a palmitoylated membrane-associated protein component of enveloped vaccinia virus. J. Virol. **77**:9008–9019.
16. **Joklik WK.** 1962. The purification of four strains of poxvirus. Virology **18**:9–18.
17. **Kates JR, McAuslan BR.** 1967. Messenger RNA synthesis by a "coated" viral genome. Proc. Natl. Acad. Sci. U. S. A. **57**:314–320.
18. **Kawauchi T, Chihama K, Nabeshima Y, Hoshino M.** 2003. The in vivo roles of STEF/Tiam1, Rac1 and JNK in cortical neuronal migration. EMBO J. **22**:4190–4201.
19. **McFadden G.** 2005. Poxvirus tropism. Nat. Rev. Microbiol. **3**:201–213.
20. **Moss B.** 2007. Poxviridae, p 2905–2946. *In* Fields BN, Knipe DM, Howley PM (ed), Virology, 5th ed, vol 2. Lippincott-Raven, Philadelphia, PA.
21. **Ploubidou A, et al.** 2000. Vaccinia virus infection disrupts microtubule organization and centrosome function. EMBO J. **19**:3932–3944.
22. **Radtke K, Dohner K, Sodeik B.** 2006. Viral interactions with the cytoskeleton: a hitchhiker's guide to the cell. Cell. Microbiol. **8**:387–400.
23. **Ridley AJ.** 2001. Rho family proteins: coordinating cell responses. Trends Cell Biol. **11**:471–477.
24. **Rietdorf J, et al.** 2001. Kinesin-dependent movement on microtubules precedes actin-based motility of vaccinia virus. Nat. Cell Biol. **3**:992–1000.

24a. **Rochester SC, Traktman P.** 1998. Characterization of the single-stranded DNA binding protein encoded by the vaccinia virus I3 gene. J. Virol. **72**:2917–2926.

25. **Roux PP, Blenis J.** 2004. ERK and p38 MAPK-activated protein kinases: a family of protein kinases with diverse biological functions. Microbiol. Mol. Biol. Rev. **68**:320–344.
26. **Sanderson CM, Way M, Smith GL.** 1998. Virus-induced cell motility. J. Virol. **72**:1235–1243.
27. **Schepis A, Schramm B, de Haan CA, Locker JK.** 2006. Vaccinia virus-induced microtubule-dependent cellular rearrangements. Traffic **7**:308–323.
28. **Schramm B, et al.** 2006. Vaccinia-virus-induced cellular contractility facilitates the subcellular localization of the viral replication sites. Traffic **7**:1352–1367.
29. **Silva PN, et al.** 2006. Differential role played by the MEK/ERK/EGR-1 pathway in orthopoxviruses vaccinia and cowpox biology. Biochem. J. **398**:83–95.
30. **Smith GL, Vanderplasschen A, Law M.** 2002. The formation and function of extracellular enveloped vaccinia virus. J. Gen. Virol. **83**:2915–2931.
31. **Soares JA, et al.** 2009. Activation of the Pi3k/Akt pathway early during vaccinia and cowpox virus infection is required for both host survival and viral replication. J. Virol. **83**:6883–6899.
32. **Togel M, Wiche G, Propst F.** 1998. Novel features of the light chain of microtubule-associated protein MAP1B: microtubule stabilization, self interaction, actin filament binding, and regulation by the heavy chain. J. Cell Biol. **143**:695–707.

33. **Tournier C, et al.** 2000. Requirement of JNK for stress-induced activation of the cytochrome c-mediated death pathway. Science **288**:870–874.
34. **Ulloa L, Avila J, Diaz-Nido J.** 1993. Heterogeneity in the phosphorylation of microtubule-associated protein MAP1B during rat brain development. J. Neurochem. **61**:961–972.
35. **Valderrama F, Cordeiro JV, Schleich S, Frischknecht F, Way M.** 2006. Vaccinia virus-induced cell motility requires F11L-mediated inhibition of RhoA signaling. Science **311**:377–381.
36. **Vivanco I, et al.** 2007. Identification of the JNK signaling pathway as a functional target of the tumor suppressor PTEN. Cancer Cell **11**:555–569.
37. **Wang F, et al.** 2004. Disruption of Erk-dependent type I interferon induction breaks the myxoma virus species barrier. Nat. Immunol. **5**:1266–1274.
38. **Wang G, et al.** 2006. Infection of human cancer cells with myxoma virus requires Akt activation via interaction with a viral ankyrin-repeat host range factor. Proc. Natl. Acad. Sci. U. S. A. **103**:4640–4645.
39. **Ward BM, Moss B.** 2001. Vaccinia virus intracellular movement is associated with microtubules and independent of actin tails. J. Virol. **75**: 11651–11663.
40. **Watanabe N, Kato T, Fujita A, Ishizaki T, Narumiya S.** 1999. Cooperation between mDia1 and ROCK in Rho-induced actin reorganization. Nat. Cell Biol. **1**:136–143.
41. **Waterman-Storer CM, Worthylake RA, Liu BP, Burridge K, Salmon ED.** 1999. Microtubule growth activates Rac1 to promote lamellipodial protrusion in fibroblasts. Nat. Cell Biol. **1**:45–50.
42. **Wittmann T, Waterman-Storer CM.** 2001. Cell motility: can Rho GTPases and microtubules point the way? J. Cell Sci. **114**:3795–3803.
43. **Wolffe EJ, Vijaya S, Moss B.** 1995. A myristylated membrane protein encoded by the vaccinia virus L1R open reading frame is the target of potent neutralizing monoclonal antibodies. Virology **211**:53–63.
44. **Woodson B.** 1968. Recent progress in poxvirus research. Bacteriol. Rev. **32**:127–137.
45. **Yang SH, Sharrocks AD, Whitmarsh AJ.** 2003. Transcriptional regulation by the MAP kinase signaling cascades. Gene **320**:3–21.